EPORT DOCUMENTATION PAGE

(2)

2a SECURITY C...	1b RESTRICTIVE MARKINGS
2b DECLASSIFICATION / DOWNGRADING SCHEDULE	3 DISTRIBUTION / AVAILABILITY OF REPORT Unlimited This document has been approved for public release and sale; its distribution is unlimited.
4 PERFORMING ORGANIZATION REPORT NUMBER(S) 13	5 MONITORING ORGANIZATION REPORT NUMBER(S)
6a NAME OF PERFORMING ORGANIZATION NIST	6b OFFICE SYMBOL (If applicable)
6c ADDRESS (City, State, and ZIP Code) A329, Materials Building Gaithersburg, MD 20899	7a NAME OF MONITORING ORGANIZATION ONR
	7b ADDRESS (City, State, and ZIP Code) Code 1131 800 N. Quincy Street Arlington, VA 22217-5000
8a NAME OF FUNDING / SPONSORING ORGANIZATION ONR	8b OFFICE SYMBOL (If applicable)
	9 PROCUREMENT INSTRUMENT IDENTIFICATION NUMBER N00014-90-F-0011
8c ADDRESS (City, State, and ZIP Code)	10 SOURCE OF FUNDING NUMBERS

PROGRAM ELEMENT NO	PROJECT NO	TASK NO	WORK UNIT NO

11 TITLE (Include Security Classification)

Growth Defects in Diamond Films

12 PERSONAL AUTHOR(S)

D. Shechtman, J.L. Hutchison, L.H. Robins, E.N. Farabaugh, and A. Feldman

13a TYPE OF REPORT	13b TIME COVERED	14 DATE OF REPORT (Year, Month, Day)	15 PAGE COUNT
Interim	FROM ____ TO ____	92-07-09	26

16 SUPPLEMENTARY NOTATION

17 COSATI CODES			18. SUBJECT TERMS (Continue on reverse if necessary and identify by block number)
FIELD	GROUP	SUB-GROUP	This document has been approved for public release and sale: its distribution is unlimited.

19 ABSTRACT (Continue on reverse if necessary and identify by block number)

Growth defects in diamond films grown by plasma-assisted chemical vapor deposition (CVD) were studied by high resolution electron microscopy. Several features of the microstructure were resolved and their importance to the growth of the diamond film was evaluated. The observations included various twin boundaries of the type $\Sigma=3$ as well as $\Sigma=9$, $\Sigma=27$ and $\Sigma=81$, which form by an interaction of lower order twins. These higher order boundaries, are loci of intersection points of growing planes on two adjacent twins and can serve as an indicator for the local crystal growth direction. The central nucleation site for the growing planes in many cases can be traced back to a quintuplet twin point. A twin quintuplet has five reentrant angles and thus serves as a preferred nucleation site for new planes as the crystal grows.

20 DISTRIBUTION / AVAILABILITY OF ABSTRACT	21 ABSTRACT SECURITY CLASSIFICATION	
☒ UNCLASSIFIED/UNLIMITED ☐ SAME AS RPT ☐ DTIC USERS	Unclassified	
22a NAME OF RESPONSIBLE INDIVIDUAL	22b TELEPHONE (Include Area Code)	22c OFFICE SYMBOL

DD FORM 1473, 84 MAR 83 APR edition may be used until exhausted
All other editions are obsolete

SECURITY CLASSIFICATION OF THIS PAGE

Enclosure (1)

OFFICE OF NAVAL RESEARCH

Contract N00014-90-F-0011

R&T Project No. IRMT 025

TECHNICAL REPORT No. 13

GROWTH DEFECTS IN DIAMOND FILMS

D. Shechtman*, J.L Hutchison**, L.H. Robins, E.N. Farabaugh, and A. Feldman

submitted to

Journal of Materials Research

National Institute of Standards and Technology

Ceramics Division

Gaithersburg, MD 20899

July 9, 1992

*Visiting scientist at the Johns Hopkins University and at NIST from the Technion, Israel.
** University of Oxford, England

GROWTH DEFECTS IN DIAMOND FILMS

D. Shechtman*
Department of Materials Engineering
Technion, Haifa, Israel

J.L. Hutchison
Oxford University, Oxford, UK

L.H. Robins, E.N. Farabaugh, and A. Feldman
National Institute of Standards and Technology**
Gaithersburg, MD 20899

ABSTRACT

Growth defects in diamond films grown by plasma-assisted chemical vapor deposition (CVD) were studied by high resolution electron microscopy. Several features of the microstructure were resolved and their importance to the growth of the diamond film was evaluated. The observations included various twin boundaries of the type $\Sigma=3$ as well as $\Sigma=9$, $\Sigma=27$ and $\Sigma=81$, which form by an interaction of lower order twins. These higher order boundaries, are loci of intersection points of growing planes on two adjacent twins and can serve as an indicator for the local crystal growth direction. The central nucleation site for the growing planes in many cases can be traced back to a quintuplet twin point. A twin quintuplet has five reentrant angles and thus serves as a preferred nucleation site for new planes as the crystal grows.

*Guest scientist at the Johns Hopkins University and at the National Institute of Standards and Technology.

**Ceramics Division, Materials Science and Engineering Laboratory, Technology Administration, U.S. Department of Commerce.

GROWTH DEFECTS IN DIAMOND FILMS

INTRODUCTION

Planar lattice defects, namely stacking faults and twins, are abundant in chemical vapor deposited (CVD) diamond structure, while diamonds that grow under thermodynamically stable conditions, such as natural diamonds, have a very low density of these defects. These differences are important to understanding the nucleation and growth of diamond films and may provide clues toward better control of microstructure and properties of CVD films.

The fine features of these growth defects can be clearly observed and studied by high resolution electron microscopy (HREM) which provides, in addition to detailed atomic resolution images, crystallographic information on the defects and their boundaries. Several reported studies on CVD diamond films[1-7] used HREM and obtained a view of the nature of stacking faults, twins and twinning configurations as well as the interface between the substrate and the diamond film.

It is the purpose of our study to closely investigate the crystallography of these defects, and, more importantly, to determine their role in the nucleation and growth of CVD diamond films.

EXPERIMENTAL

SPECIMEN PREPARATION

The fabrication of the free-standing CVD diamond films used in this study has been discussed in a previous article[8]. The deposition was made by microwave plasma assisted CVD on a commercial silicon wafer. In order to promote diamond nucleation, defects were introduced onto the polished surface of the substrate by rubbing with 1 μm diamond powder. The deposition conditions are given in Table 1.

The diamond grain size was about 0.1 μm and optical reflectance measurements suggest that the root mean square surface roughness of these films is approximately 0.02 μm. Following deposition, the substrate was etched away chemically and squares 3 mm on a side, were cut from the film. The diamond squares were then placed between electron microscope grids and thinned by ion milling.

ELECTRON MICROSCOPY

A high resolution electron microscope at Oxford University, England was used in this study. The microscope features an objective lens with a spherical aberration coefficient of

C_s=0.9 mm and it operates at 400 kV. The point resolution is 0.16 nm giving accurate transmission of {111} and {200} diamond reflections into the image. The information limit is 0.12 nm so that {220} reflections also contribute to the image contrast. The crystals were tilted into an exact <110> orientation for high resolution image recordings and a 500k magnification was used close to the Scherzer defocus (-48 nm).

RESULTS AND DISCUSSION

TYPE OF DIAMOND TWINS

A list of the twin boundaries that have been found in this study of the diamond lattice and the respective lattice rotation angles is given in Table 2. The coincidence site lattice notation is used[9].

Σ=3 TWIN BOUNDARIES

Twin boundaries of the Σ=3 type have been observed in natural, artificial and thin film diamond layers as well as in other materials that have the diamond lattice. Examples include silicon[10-12] and diamond[13]. The twins are of the {111} type and in all cases are formed during the crystal growth. This is in contrast to deformation twins, which occur when a material undergoes deformation as a result of high internal stresses. The important twinning planes and directions in the diamond lattice are shown in the high resolution micrograph seen in figure 1. The twinning plane k_1 in this example is $(1\bar{1}1)$. The rest of the twinning elements are:

k_2 - $(\bar{1}11)$
η_1 - $[\bar{1}12]$
η_2 - $[1\bar{1}2]$
} in the matrix coordinate system.

k'_2 - $(1\bar{1}\bar{1})$
η'_2 - $[1\bar{1}2]$
} in the twin coordinate system.

This is illustrated in the double stereographic projection, figure 2, in which the twin planes (and directions) are marked with open circles ○ while those of the matrix are marked by solid circles ●.

The twinned region in figure 1 has a high volume fraction of twins. This is not usually the case in other regions examined but it clearly indicates that the {111} twins can be readily formed and that the orientation of the crystal can switch back and forth with little energy penalty. The stacking fault energy and thus the twinning energy are apparently relatively small in diamond.

A diffraction pattern from a twinned region and its analysis are shown in figure 3.

The twin and matrix diffraction spots are marked ○ and ●, respectively. There are a large number of forbidden reflections that appear in the pattern. (See Table 3 about the structure factor which determines the allowed and forbidden reflections.) The forbidden reflections are due to double diffraction generated at the twin-matrix boundaries[14]. The streaks seen in the pattern originate from narrow twins and lie in a direction normal to the twin plane, ie. <111>.

TWIN BOUNDARIES OF HIGHER ORDER

Figure 4 illustrates the types of twins found in the film. The zone axis of the reflecting planes of all the twins seen in this part of the crystal is of the <110> type; the two edge-on {111} planes in each twin are indicated in the figure. The simplest twin boundary is seen in the lower right corner of the micrograph. This is a $\Sigma=3$ twin boundary of which the lower and the upper parts are coherent (the twin mirror plane and the twin boundary coincide) while the middle part is noncoherent. The noncoherent part of the boundary follows a (111) plane of only one of the twins, thus it is not a K_1 plane. $\Sigma=3$ twins are abundant in CVD diamond and are usually coherent. It is the intersection of these twin boundaries that cause the formation of the higher order boundaries. An example of such a higher order boundary is shown in figure 4 extending from the upper right to the left. This boundary divides the field of view into two parts, the upper, marked I, has only two $\Sigma=3$ boundaries bounding a narrow twin, while the lower part, marked II has several boundaries of this type. In order to illustrate the interaction among the twins, we shall start by examining the $\Sigma=9$ boundary between point A and B. This part of the boundary is a $\Sigma=9$ type except at the short segments marked A' and A" where it intersects with two narrow twins. The rotation angle between part I and II along this part of the boundary is measured to be about 39° thus fitting the criterion for a $\Sigma=9$ boundary. The boundary extends near a (111) plane of twin II and shifts, at point A", to a surface close to a (111) of twin I. This $\Sigma=9$ boundary intersects a $\Sigma=3$ boundary at point A, creating a $\Sigma=27$ boundary, which has a rotation angle of about 32° as measured on the micrograph. The $\Sigma=27$ boundary extends on a surface that does not seem to relate to any specific lattice plane.

At the upper right side of figure 4 at point B, the $\Sigma=9$ boundary intersects two $\Sigma=3$ twins to form a $\Sigma=81$ boundary with a rotation angle of about 78°. This type of boundary is sensitive to the orientation of the lattice; the {111} planes of the twins on the opposite sides of the boundary are nearly parallel (7.356° apart). This $\Sigma=81$ boundary transforms into a coherent $\Sigma=3$ boundary at point C by a series of dislocations on the {111} planes along both of its sides between point B and C.

While it is takes a rather straight-forward procedure to analyze the various twin boundaries in their edge-on positions, as seen in figure 3, a computer simulation may be needed to recognize boundaries which are tilted away from an edge-on position. Such is the case demonstrated in figure 5. In this example, $\Sigma=3$ boundaries intersect to form a $\Sigma=9$ boundary as marked on the micrograph. The nature of the orientation relationship between

the upper portion of the crystal, marked I and the lower, marked II, can be characterized as $\Sigma=3$ between I and IIa while the one between I and IIb is of the $\Sigma=9$ type. The boundaries shown are therefore $\Sigma=3$ and $\Sigma=9$, respectively. The contrast of the tilted boundaries varies as the tilt angle changes but the characteristic symmetry remains the same. A systematic computer simulation is needed in order to recognize the contrast effects in the various tilt angles.

We will deal now with some details of the $\Sigma=3$ twin boundaries and characteristic formations observed in the diamond lattice.

CHARACTERISTIC TWIN BOUNDARY FORMATIONS

The "V" Shape Formation: Figure 6 presents a $\Sigma=3$ twin interaction in which two such twins form a $\Sigma=9$ boundary that extends between them. The angle between the twin boundaries is identical to the angle between the two {111} planes of the lattice, i.e. 70.529°. This $\Sigma=9$ boundary forms on a surface that is the locus of intersection points of growing planes on two adjacent parts of the crystal. It thus indicates the crystal growth direction in that vicinity and the "V" shape formation can therefore indicate not only the local growth direction but can also help us trace back to the starting point of growth in the specific crystal cut that makes up the TEM foil.

The "V" formation is rather abundant in the diamond film as can be seen in figure 7. The hollow arrows which point at the "V" formations also indicate the local growth directions which are logically directed toward the outer surface of the crystal, a part of which is seen in this micrograph.

Tracing back to the nucleation site of the growing planes in this cross-section of the crystal may be the most useful role that the "V" formations play in our understanding of diamond crystal growth. Illustrated in figure 8 is a cross-section of a small crystal on which the "V" formations as well as a higher order twin boundary are marked. If we follow the growth path backwards from the surface to the inside of the crystal, we can identify the nucleation site to be a twin quintuplet center. The importance of the twin quintuplet site to the nucleation and growth of CVD diamond crystals will be discussed later in the text.

Twin Quintuplets: A closer look at a twin quintuplet is shown in figure 9. In this case, five $\Sigma=3$ twins meet at a point and the formation of a 7.356° misfit angle is illustrated in the inset. A $\Sigma=81$ boundary is thus formed. Our observations indicate that in most cases, a twin quintuplet center is surrounded by four $\Sigma=3$ boundaries and one $\Sigma=81$ boundary. In other cases we have observed that two misfit angles, the sum of which is 7.356°, broaden two of the otherwise $\Sigma=3$ boundaries. In such cases the center point is surrounded by three $\Sigma=3$ and two deformed $\Sigma=3$ boundaries.

Higher Order Boundaries: Crystal grains that contain $\Sigma=3$ twins have been observed in materials having the diamond lattice. Several examples include silicon[10-12] and diamond[13].

Higher order boundaries (Σ=9, Σ=27 and Σ=81) have been studied less, but, they provide a key to understanding the growth of diamond CVD crystals. This is because high order boundaries are the locus of the points of intersection of growing planes from two adjacent twins of order greater than Σ=3. The boundaries are aligned, therefore, along the local growth direction of the crystal and allow, like the "V" shape formations, the determination of the growth directions at various points of the crystal as well as the nucleation point of the growing planes in the TEM cross-section. An example of such a determination is shown, as mentioned before, in figure 8.

THE ROLE OF TWINNING IN THE GROWTH OF CVD DIAMOND

A large number of diamond grains have been investigated in the course of our study. In all cases the grains were twinned and the distribution of the twins was irregular. Since twinning is very common, it seems that twins play an important role in the growth of CVD diamond crystals.

The importance of twins to the growth of germanium has been studied in the past and consequently utilized to promote the growth of germanium dendrites from the melt[15-19]. The model of Hamilton and Seidensticker[17], which utilizes the Σ=3 twin boundary reentrant angle (141° between the nonparallel {111} plane in the adjacent twins) to explain crystal growth, has shed light on the vital importance of twinning to rapid growth of germanium. The model for fast growth calls for a pair of parallel Σ=3 twin boundaries that form a new reentrant angle as one twin boundary ceases to serve as a preferred growth site. In the case that only one twin boundary is present, a bicrystalline trigonal solid is formed provided that all three reentrant corner sites are allowed to grow.

While twins serve a crucial role in the growth of germanium crystals, this does not seem to be the case in the growth of silicon crystals. Twinned silicon crystals have been grown from the melt[20], but it is not clear that twins cause fast growth as in the case of germanium. In other metals and intermetallics, twins serve as a preferred sites for the growth of dendrites. One such example is the growth of cadmium crystals[21]. However, we will not discuss this case and limit ourselves to crystals with diamond cubic structure.

A key to understanding the role of twinning in the growth of diamond crystals in the CVD process is an examination of the stability of a carbon atom attached to a given point on the surface of a growing crystal. During the formation of natural diamonds (see reference [22] for example) or in commercial high-temperature high-pressure processes, growth does not occur in a reactive environment as in the case of CVD growth. A carbon atom attached to a free surface of the growing crystals under equilibrium growth conditions is relatively stable and can stay in position, thus forming a preferred site for the formation of a new {111} plane. In CVD diamond growth, it is likely that such an atom would be etched away by the atomic hydrogen. The harsher the CVD conditions are, the more faceted he diamond crystals become. Carbon atoms that position themselves in a reentrant angle site will be

more stable. When a new plane forms at the reentrant site, it can grow rapidly because there are stable positions at the step site of the propagating plane. The reentrant site between twins can shoot out propagating planes rapidly at a rate that controls the local growth rate (figure 10). The local growth is on adjacent {111} planes, but, on a larger scale the crystal grows in the <211> directions. A demonstration of the effect of twinning on growth in the diamond cubic structure is given by Hamilton and Seidensticker[17].

Five $\Sigma=3$ twin boundaries, at the most, can meet at a point on a plane, and usually (as discussed above) one of them is actually a $\Sigma=81$ boundary (see figure 10). A twin quintuplet is therefore a favorable nucleation site for new planes, mainly due to the five 141° reentrant angles around the 5-fold axis (see figure 9).

The maximum number of $\Sigma=3$ twins that can form around a point in space is 20 and an icosahedron forms as they grow. The icosahedron has 12 twin quintuplets (five-fold axes) and 30 reentrant angle sites serving therefore as a superior nucleation site for the whole of a crystal. During this study we have observed a large number of icosahedral diamond crystals on the first layer formed. This may explain why many of the observed CVD crystals are icosahedral in shape, and the cross-sections exhibit one or more twin quintuplet axes.

Following the proposed growth model (see figure 10) it is expected that the vertices (5-fold axes) and in certain cases the edges (2-fold axes) of such twinned icosahedrons will be grooved since they provide the nucleation sites for the new planes. Indeed, this is the case as illustrated in figure 11. In fact, such grooves are expected to form also in cases when only fractions of the icosahedron develop.

CONCLUSION

This study by high resolution electron microscopy of plasma assisted CVD diamond films has centered on the determination of twinning parameters and the role of twins in the growth of diamond crystals under the characteristic metastable conditions typical to the CVD technique. We have shown that the various configurations of twins can indicate the growth direction in certain parts of the diamond crystal, thus helping us determine the origin of the growing planes in various cross-sections of the crystal. We have also shown that the reentrant angle between twins is a preferred nucleation site for growing planes and that a twin quintuplet is thus a superior growth center, because it contains the maximum number of reentrant angles that can meet at a point. The icosahedral shape of a large number of twinned diamond crystals and the grooves along the vertices (5-fold axes) and along the edges (2-fold axes) are explained by this study and are consistent with an icosahedral cage compound precursor nucleation site[23].

ACKNOWLEDGEMENT

This work was supported in part by the Office of Naval Research. The assistance of the Louis Edelstein Center of the Technion is gratefully acknowledged.

REFERENCES

1. B.E. Williams and J.T. Glass, J. Mater. Res. 4, 373 (1989).

2. J. Narayan, J. Mater. Res. 5, 2414 (1990).

3. B.E. Williams, J.T. Glass, R.F. Davis, K. Kobashi and K.L. More, Proc. 1st Int. Symp. Diamond and Diamond Like Films, J.P. Dismukes, editor 202 (1989).

4. G-H.M. Ma, Y.H. Lee and J.T. Glass, J. Mater. Res. 5, 2367 (1990).

5. J. Narayan, A.R. Srivatsa, M. Peters S. Yokota and K.V. Ravi, Appl. Phys. Lett. 53, 1823 (1988).

6. B.E. Williams, H.S. Kong and J.T. Glass, J. Mater. Res. 5, 801 (1990).

7. K. Kobashi, K. Nishimura, K. Miyata, Y. Kawate, J.T. Glass and B.E. Williams, SPIE Diamond Optics, 969, 159 (1988).

8. D. Shechtman, E.N. Farabaugh, L.H. Robins and J.L. Hutchison SPIE Diamond Optics IV, 1534, 26 (1991).

9. S. Ranganathan, Acta Cryst. 21, 197 (1966).

10. M.D Vaudin, B. Cunningham and D.G. Ast, Scripta Met. 17, 191 (1983).

11. S. Iijima, Jpn. J. Appl. Phys. 26, 357 (1987).

12. S. Iijima, Jpn. J. Appl. Phys. 26, 365 (1987).

13. U. Dahmen, C.J. Hetherington, P. Piruz and K.H. Westmacott, Scripta Met. 23, 269 (1989).

14. P.B. Hirsch, A. howie, R.B. Nicholson, D.W. Pashley and M.J. Whelan, Electron Microscopy of Thin Crystals, Butterworths, London, (1967).

15. R.S. Wagner, Acta Met. 8, 57 (1958).

16. A.I.Bennett and R.L.Longini, Phys. Rev. 116, 53 (1959).

17. D.R. Hamilton and R.G. Seidensticker, J. Appl. Phys. 31, 1165 (1960).

18. D.R. Hamilton and R.G. Seidensticker, J. Appl. Phys. 34, 1450 (1963).

19. R.G. Seidensticker and D.R. Hamilton, J. Appl. Phys. 34, 3113 (1963).

20. T. Abe, J. Crystal Growth 24/25, 463 (1974).

21. P.B. Price, Phil. Mag. 4, 1229 (1960).

22. A.R. Lang, J. Crystal Growth 24/25, 108 (1974).

23. S. Matsumoto and Y. Matsui, J. Mater. Sci. 18, 1785 (1983).

Table 1. Deposition conditions

Microwave power - 1kW
Graphite susceptor temperature - 650 °C
The temperature of the growing film is known to be considerably higher as a result of the heating in the microwave plasma.
Gas pressure - 6.6×10^3 Pa
Gas flow rate - 260 standard cm^3/min
Gas composition - 99.5% H_2, 0.5% CH_4
Deposition time - 45 min
Growth rate - 0.4 μm/h
Total thickness - 0.3 μm

Table 2. Diamond lattice twin boundaries

Twin Type (Coincidence Lattice Site Notation)	Twinning Angle (Degrees))
$\Sigma=3$	70.529
$\Sigma=9$	38.942
$\Sigma=27$	31.586
$\Sigma=81$	77.885

Table 3. The Structure Factor, F, as a Function of the Atomic Scattering Factor, f. The parameters (h, k, l) are the Miller indices of the reflecting plane. When F=0, a reflection is forbidden.

(h+k+l) odd	$\|F\|^2=32f^2$
(h+k+l) even multiple of 2	$\|F\|^2=64f^2$
(h+k+l) odd multiple of 2	$\|F\|^2=0$

FIGURE CAPTIONS

Figure 1. A twinned region in a diamond foil. The main twinning elements are marked on the micrograph.

Figure 2. The twinning elements of the twin shown in figure 1.

Figure 3. A diffraction pattern from a twinned part of the crystal (left) and the analysis of the diffraction pattern (right).

Figure 4. Twin boundaries found in CVD diamond films.

Figure 5. Twin boundaries of types $\Sigma=3$ and $\Sigma=9$ that are tilted with respect to the electron beam. The angles indicate the orientations of local {111} axes.

Figure 6. The $\Sigma=9$ boundary at [B] between the two $\Sigma=3$ twin boundaries forms on a surface that is the locus of intersection points of growing planes on the two adjacent T_2 and T_3 twins.

Figure 7. Higher order boundaries (all arrows) are more frequently found in the periphery of the crystal. Hollow arrows indicate the local growth direction of the crystal.

Figure 8. Cross-section of a complete crystal. Growth directions are indicated by the arrows; thus, tracing in the opposite direction can aid us in finding the nucleation site of the growing planes. Here, the nucleation site is the twin quintuplet indicated by the circle on the micrograph.

Figure 9. Micrograph showing a twin quintuplet (marked A). A high order twin boundary of type $\Sigma=81$ is formed which shows a 7.5° mismatch of a set of {111} planes in the crystals on opposite sides of the boundary (see inset). The geometry of higher order boundaries and its importance are discussed in the text.

Figure 10. The growth of a (111) plane starts at points along the 141° reentrant corner.

Figure 11. The grooves along the 2-fold edges and the indentation in the 5-fold vertices result from the growth mechanism described in the text. The grooves are commonly found along the intersections of twin habit planes and the surface of the growing diamond crystals.

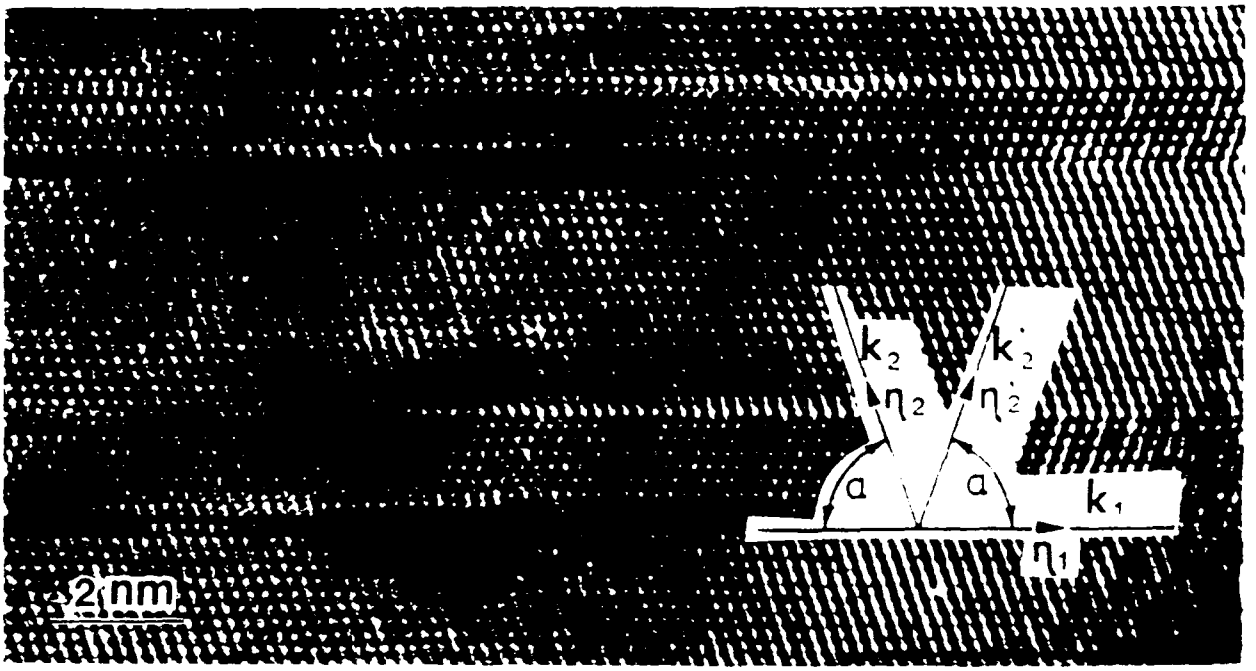

FIGURE 1 A twinned region in the diamond foil. The main twinning elements are marked on the micrograph.

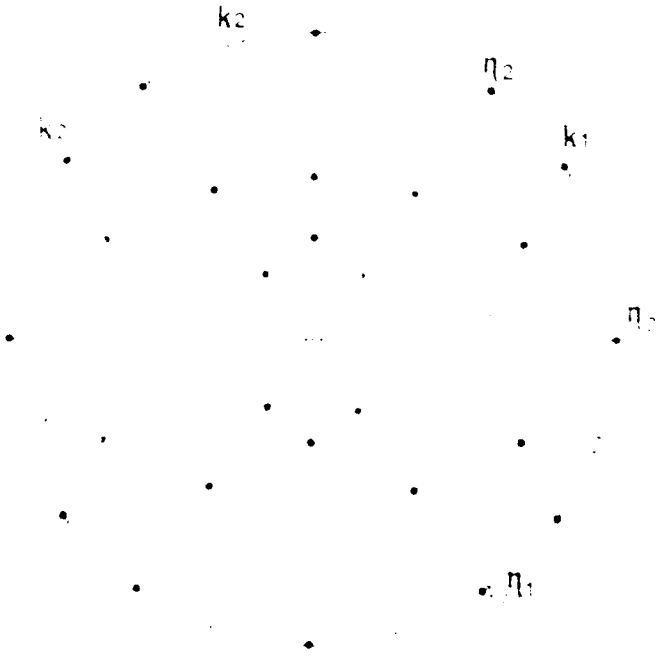

FIGURE 2 The twinning elements of the twin shown in figure 1.

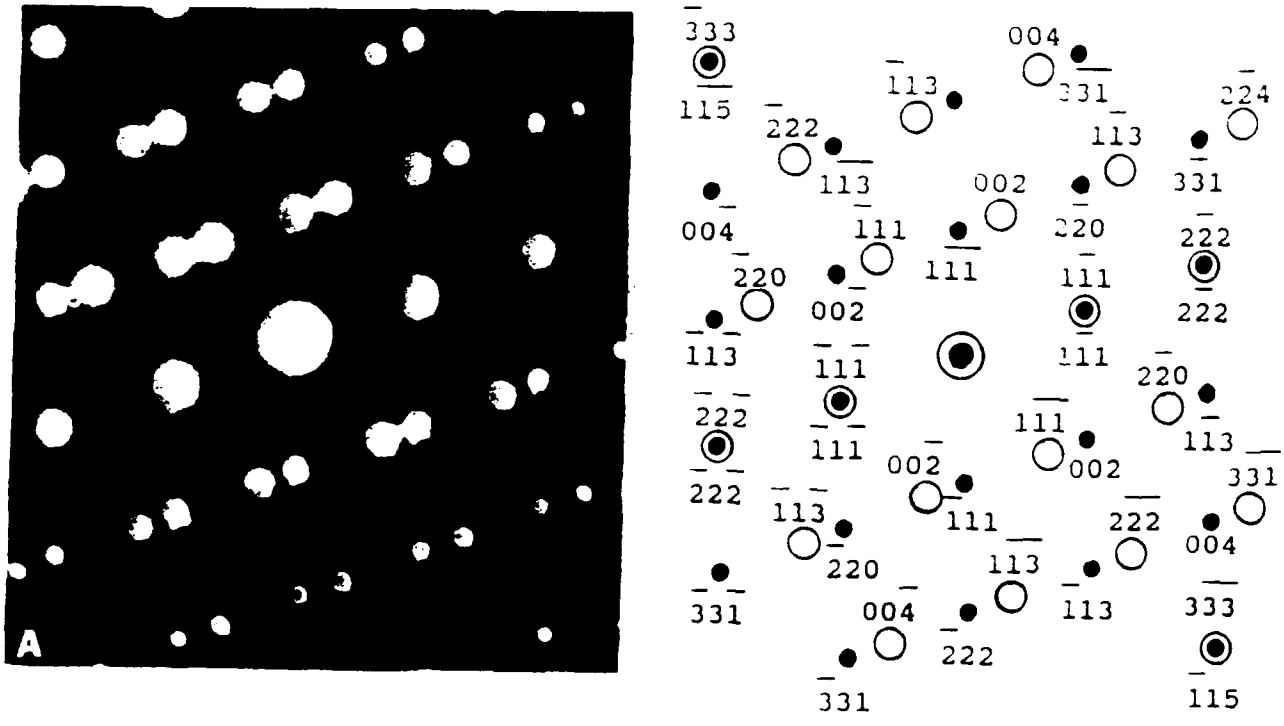

Figure 3. A diffraction pattern from a twinned part of the crystal (left) and the analysis of the diffraction pattern (right).

Figure 4 Twin boundaries found in CVD diamond films.

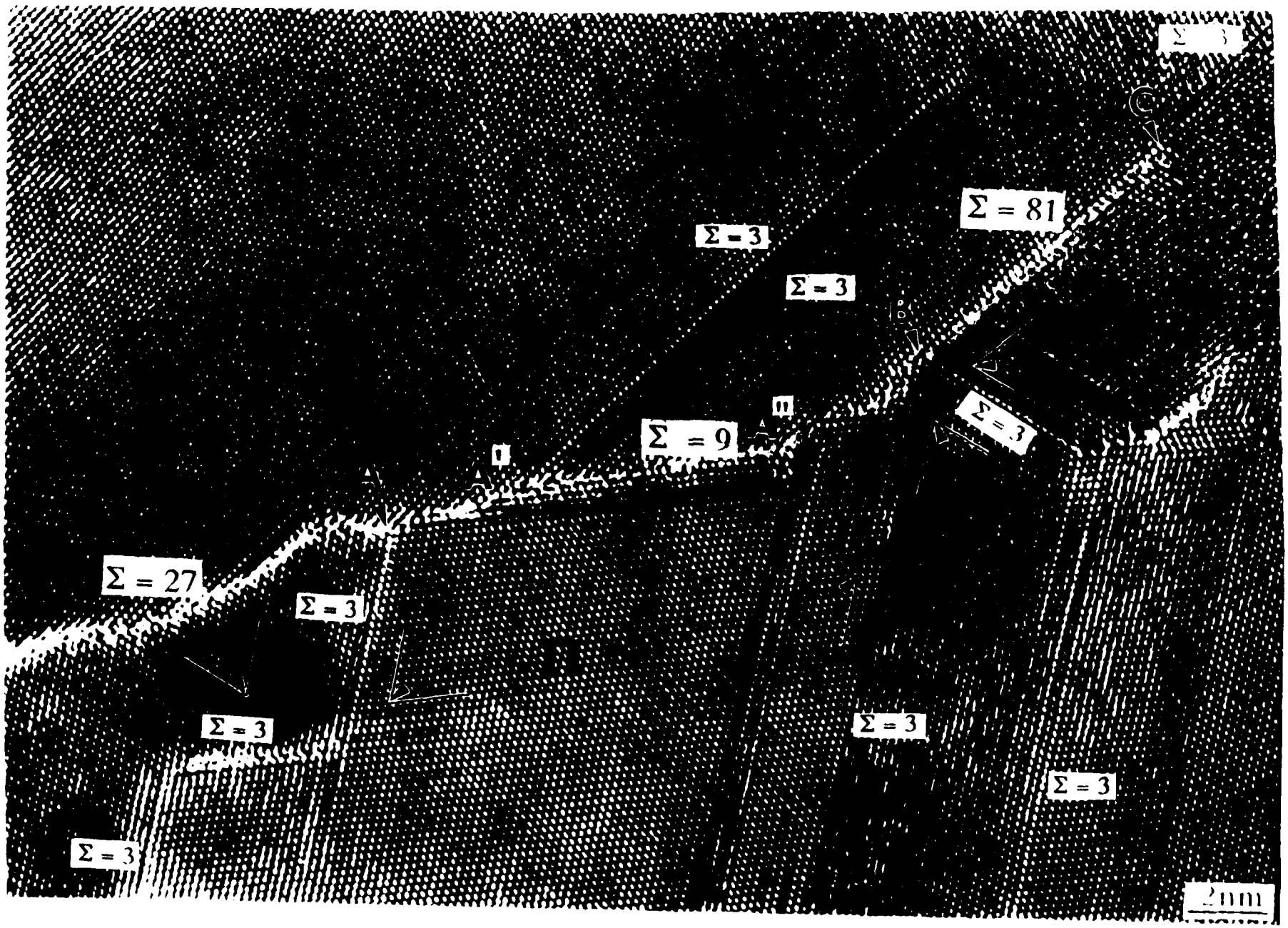

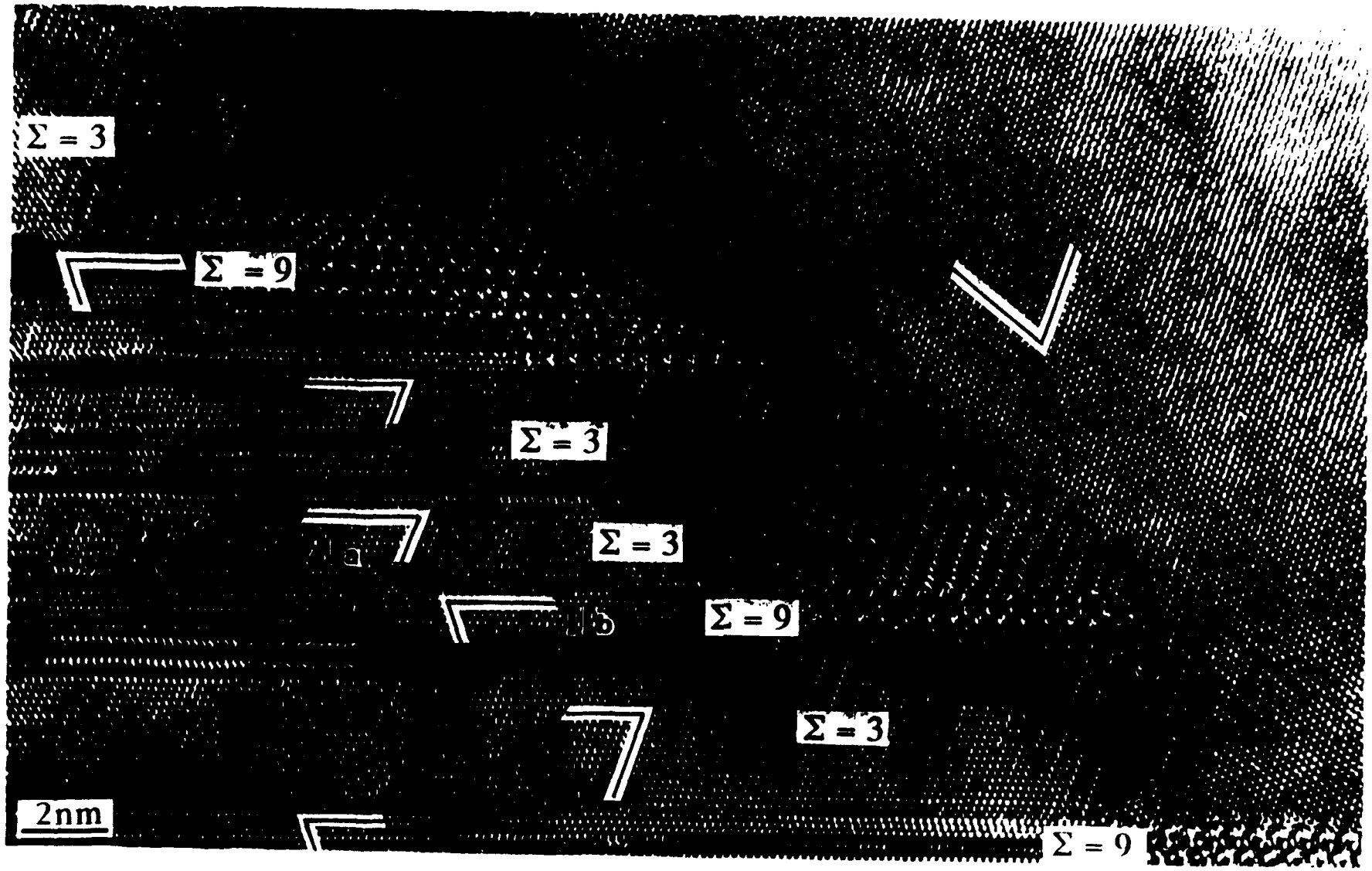

Figure 5. Twin boundaries of types $\Sigma=3$ and $\Sigma=9$ that are tilted with respect to the electron beam. The angles indicate the orientations of local {111} axes.

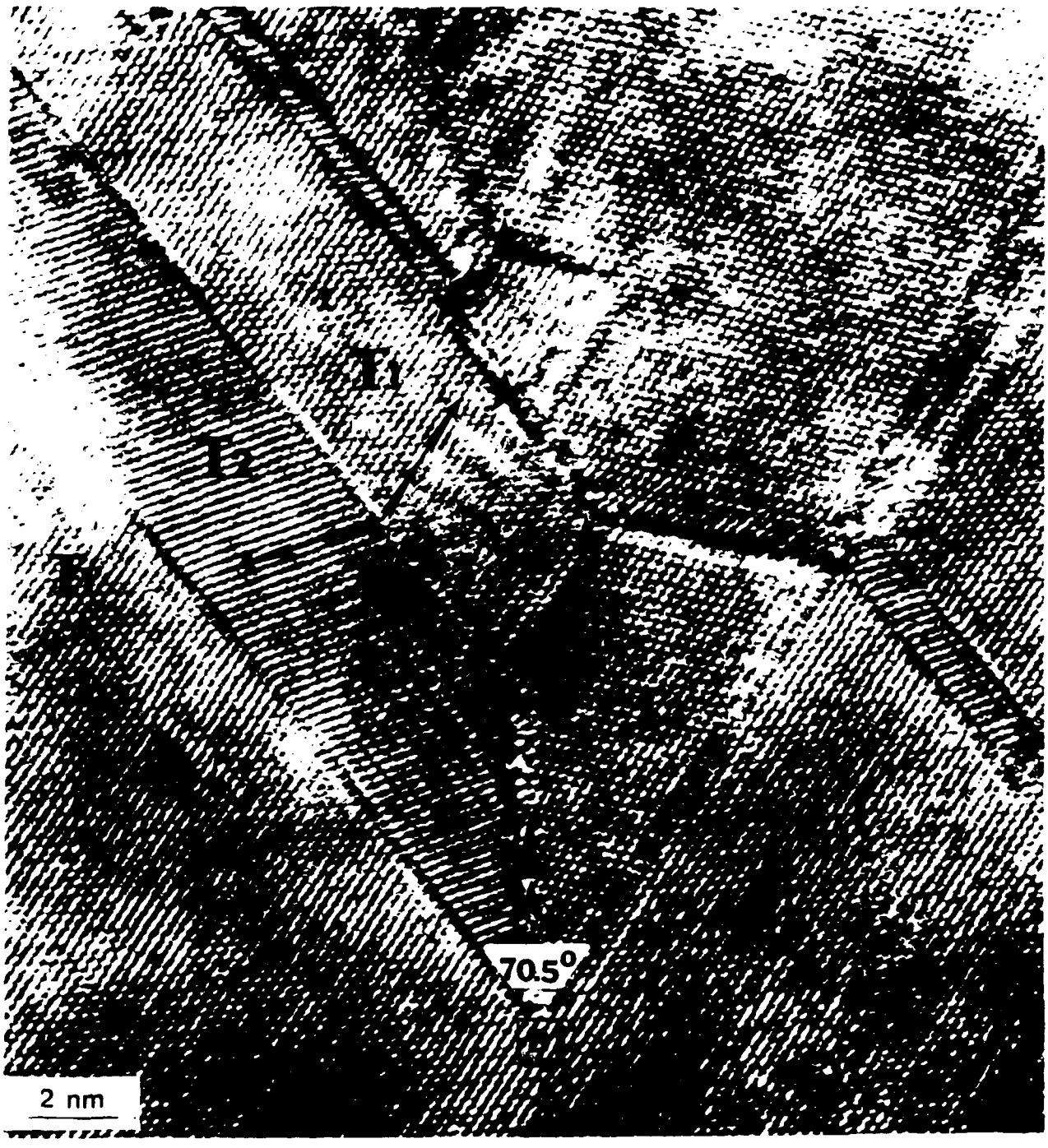

Figure 6. The $\Sigma=9$ boundary at [B] between the two $\Sigma=3$ twin boundaries forms on a surface that is the locus of intersection points of growing planes on the two adjacent T_2 and T_1 twins.

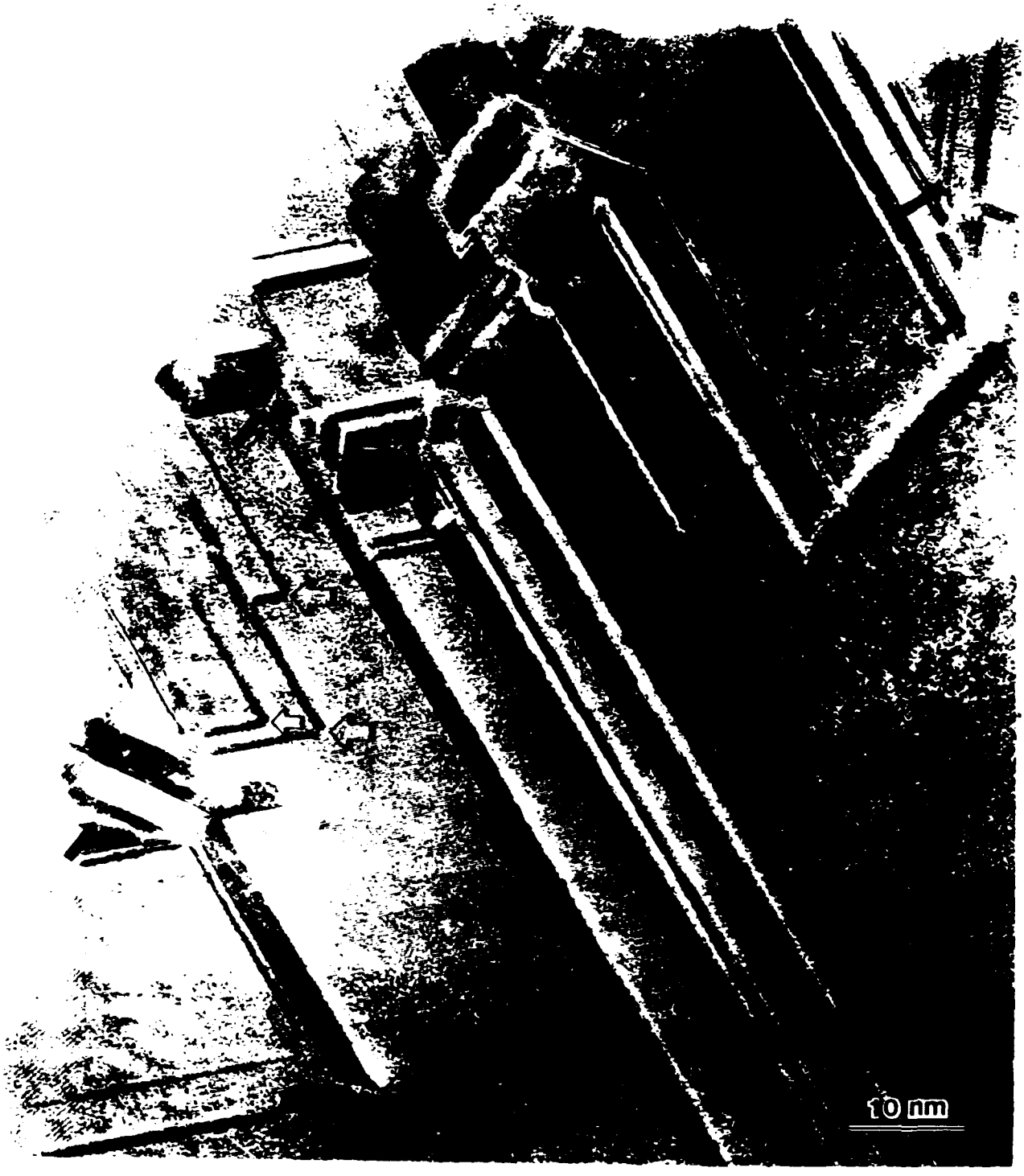

Figure 7. High order twin boundaries (all arrows) are more frequently found in the periphery of the crystal. Hollow arrows indicate also the local growth direction of the crystal.

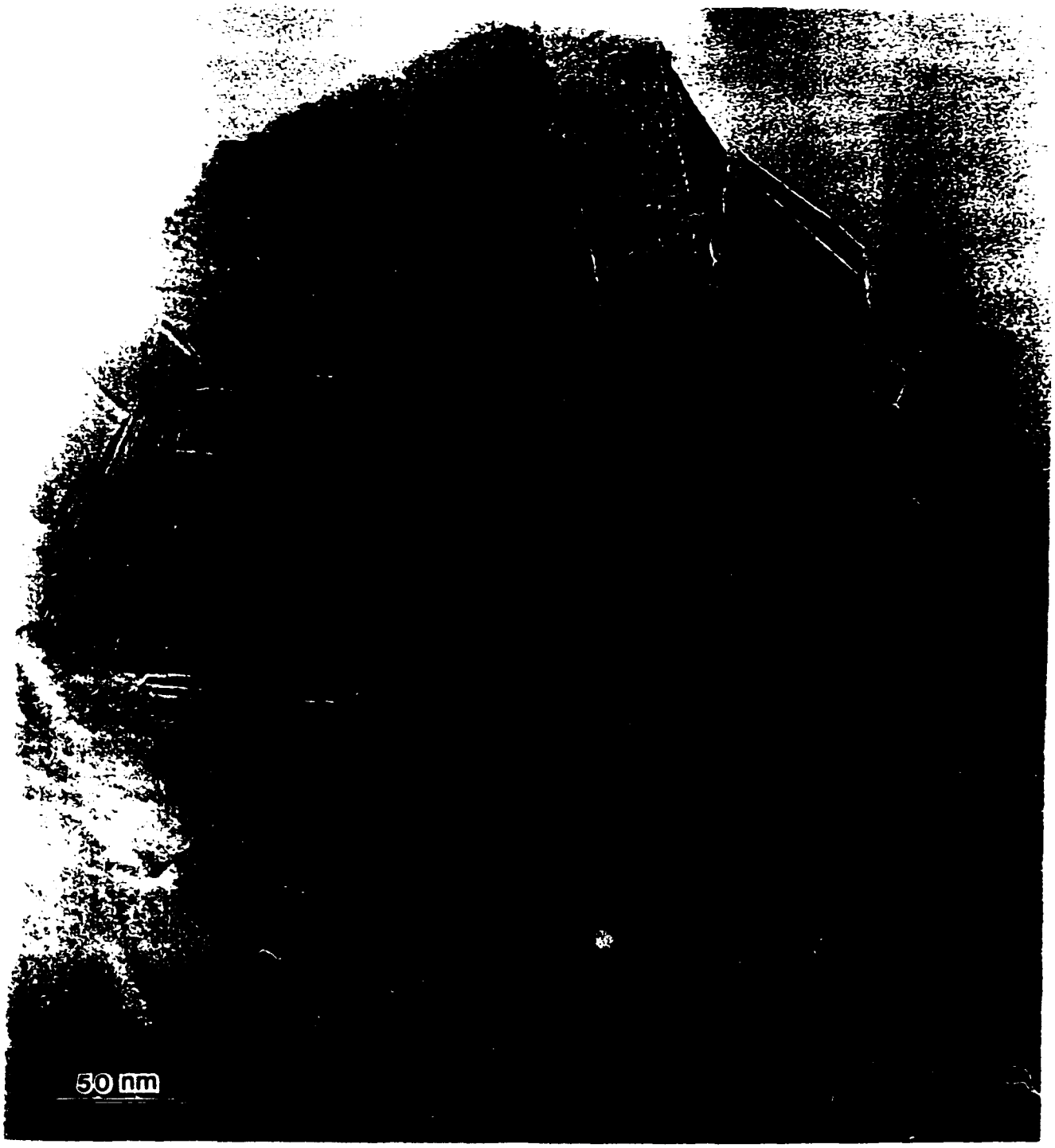

Figure 8. Cross-section of a complete crystal. Growth directions are indicated by the arrows; thus, tracing in the opposite direction can aid us in finding the nucleation site of the growing planes. Here, the nucleation site is the twin quintuplet indicated by the circle on the micrograph.

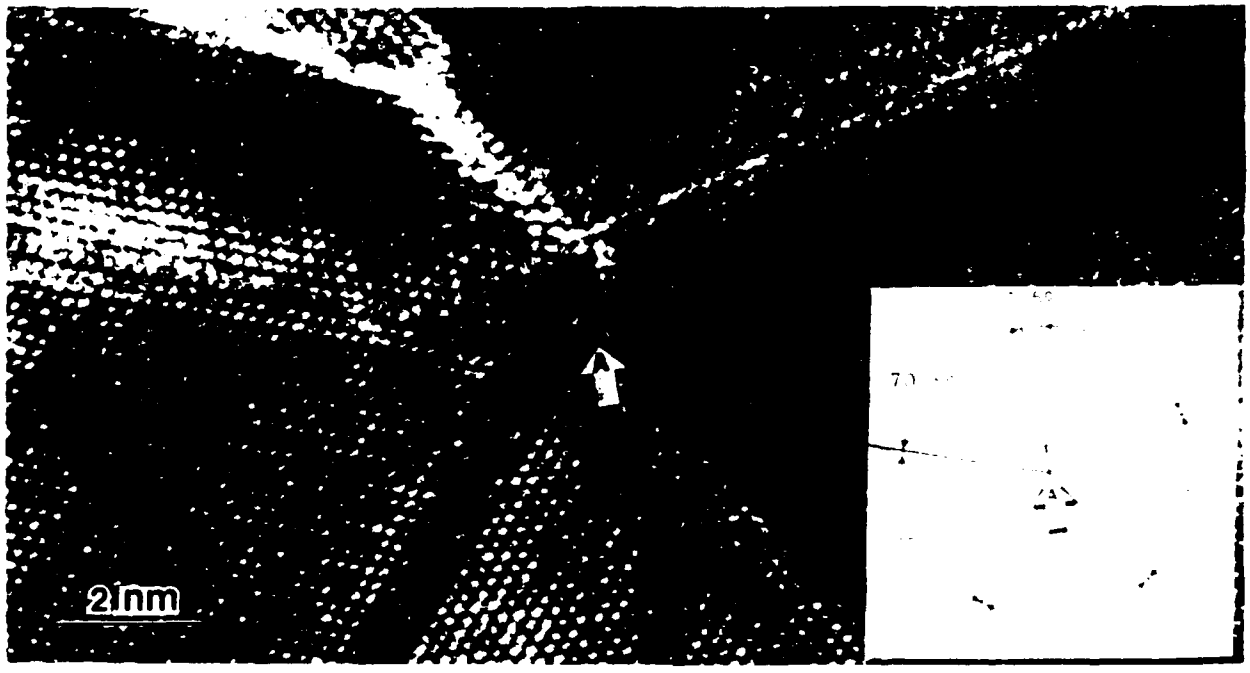

Figure 9. Micrograph showing a twin quintuplet (marked A). A high order twin boundary of type $\Sigma=81$ is formed which shows a 7.5° mismatch of a set of {111} planes in the crystals on opposite sides of the boundary (see inset). The geometry of higher order boundaries and its importance are discussed in the text.

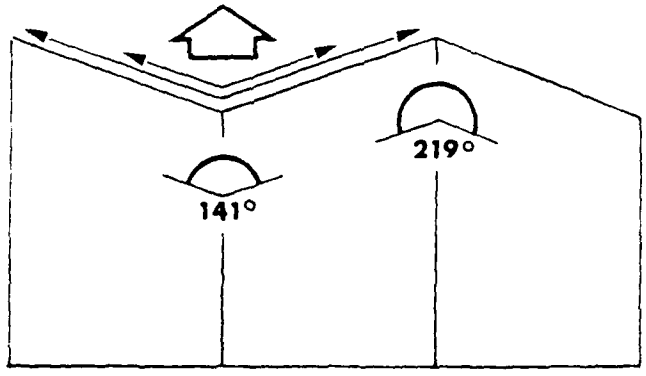

Figure 10. The growth of a (111) plane starts at points along the 141° reentrant corner.

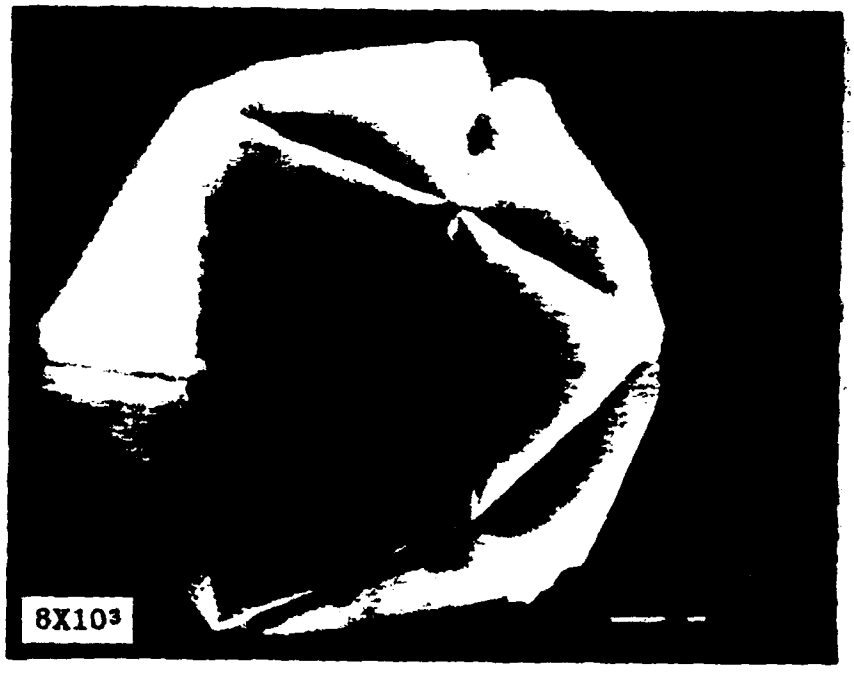

Figure 11. The grooves along the 2-fold edges and the indentation in the 5-fold vertices result from the growth mechanism described in the text. The grooves are commonly found along the intersections of twin habit planes and the surface of the growing diamond crystals.

27 June 1992

Distribution List

Mr. James Arendt
Hughes Aircraft Company
8433 Fallbrook Avenue 270/072
Canoga Park, CA 91304
(838) 702-2890

Mr. Larry Blow
General Dynamics
1525 Wilson Blvd., Suite 1200
Arlington, VA 22209
(703) 284-9107

Mr. Ellis Boudreaux
Code AGA
Air Force Armament Laboratory
Eglin AFB, FL 32542

Dr. Duncan W. Brown
Advanced Technology Materials, Inc.
7 Commerce Drive
Danbury, CT 06810-4131

Dr. Mark A. Cappelli
Stanford University
Mechanical Engineering Department
Stanford, CA 94305
(415) 723-1745

Dr. R. P. H. Chang
Materials Science & Engineering Dept.
2145 Sheridan Road
Evanston, IL 60208
(312) 491-3598

Defense Documentation Center
Cameron Station
Alexandria, VA 22314
(12 copies)

Dr. Bruce Dunn
UCLA
Chemistry Department
Los Angeles, CA 90024
(213) 825-1519

Dr. Al Feldman
Leader, Optical Materials Group
Ceramics Division
Materials Science & Engineering Lab
NIST
Gaithersburg, MD 20899
(301) 975-5740

Dr. John Field
Department of Physics
University of Cambridge
Cavendish Laboratory
Madingley Road
Cambridge CB3 OHE
England
44-223-3377333 Ext. 7318

Dr. William A. Goddard, III
Director, Materials and Molecular
Simulation Center
Beckman Institute
California Institute of Technology
Pasadena, CA 91125
(818) 356-6544 Phone
(818) 568-8824 FAX

Dr. David Goodwin
California Institute of Technology
Mechanical Engineering Dept.
Pasadena, CA 91125
(818) 356-4249

Dr. Kevin Gray
Norton Company
Goddard Road
Northboro, MA 01532
(508) 393-5968

Enclosure (1)

Mr. Gordon Griffith
WRDC/MLPL
Wright-Patterson AFB, OH 45433

Dr. H. Guard
Office of Chief of Naval Research
(ONR Code 1113PO)
800 North Quincy Street
Arlington, VA 22217-5000

Dr. Alan Harker
Rockwell Int'l Science Center
1049 Camino Dos Rios
P.O. Box 1085
Thousand Oaks, CA 91360
(805) 373-4131

Mr. Stephen J. Harris
General Motors Research Laboratories
Physical Chemistry Department
30500 Mound Road
Warren, MI 48090-9055
(313) 986-1305 Phone
(313) 986-8697 FAX
E-mail: SHARRIS@GMR.COM

Mr. Rudolph A. Heinecke
Standard Telecommunication
Laboratories, Ltd.
London Road
Harlow, Essex CM17 9MA
England
44-279-29531 Ext. 2284

Dr. Kelvin Higa
Code 3854
Naval Weapons Center
China Lake, CA 93555-6001

Dr. Curt E. Johnson
Code 3854
Naval Weapons Center
China Lake, CA 93555-6001
(619) 939-1631

Dr. Larry Kabacoff (Code R32)
Officer in Charge
Naval Surface Weapons Center
White Oak Laboratory
10901 New Hampshire
Silver Spring, MD 20903-5000

Mr. M. Kinna
Office of Chief of Naval Research
(ONT Code 225)
800 North Quincy Street
Arlington, VA 22217-5000

Dr. Paul Klocek
Texas Instruments
Manager, Advanced Optical Materials Br.
13531 North Central Expressway
P.O. Box 655012, MS 72
Dallas, TX 75268
(214) 995-6865

Ms. Carol R. Lewis
Jet Propulsion Laboratory
4800 Oak Grove Drive
Mail Stop 303-308
Pasadena, CA 91109
(818) 354-3767

Dr. J.J. Mecholsky, Jr.
University of Florida
Materials Science & Engineering Dept.
256 Rhines Hall
Gainesville, FL 32611
(904) 392-1454

Dr. Russell Messier
202 Materials Research Laboratory
Pennsylvania State University
University Park, PA 16802
(814) 865-2326

Mr. Mark Moran
Code 3817
Naval Weapons Center
China Lake, CA 93555-6001

Mr. Ignacio Perez
Code 6063
Naval Air Development Center
Warminster, PA 18974
(215) 441-1681

Mr. C. Dale Perry
U.S. Army Missile Command
AMSMI-RD-ST-CM
Redstone Arsenal, AL 35898-5247

Mr. Bill Phillips
Crystallume
125 Constitution Drive
Menlo Park, CA 94025
(415) 324-9681

Dr. Rishi Raj
Cornell University
Materials Science & Engineering Dept.
Ithaca, NY 14853
(607) 255-4040

Dr. M. Ross
Office of Chief of Naval Research
(ONR Code 1113)
800 North Quincy Street
Arlington, VA 22217-5000

Dr. Rustum Roy
102A Materials Research Laboratory
Pennsylvania State University
University Park, PA 16802
(814) 863-7040 FAX

Dr. James A. Savage
Royal Signals & Radar Establishment
St. Andrews Road
Great Malvern, Worcs WR14.3PS
England
01-44-684-895043

Mr. David Siegel
Office of Chief of Naval Research
(ONT Code 213)
800 North Quincy Street
Arlington, VA 22217-5000

Dr. Keith Snail
Code 6520
Naval Research Laboratory
Washington, DC 20375
(202) 767-0390

Dr. Y. T. Tzeng
Auburn University
Electrical Engineering Department
Auburn, AL 36849
(205) 884-1869

Dr. Terrell A. Vanderah
Code 3854
Naval Weapons Center
China Lake, CA 93555-6001
(619) 939-1654

Dr. George Walrafen
Howard University
Chemistry Department
525 College Street NW
Washington, DC 20059
(202) 806-6897/6564

Mr. Roger W. Whatmore
Plessey Research Caswell Ltd.
Towcester Northampton NN128EQ
England
(0327) 54760

Dr. Charles Willingham
Raytheon Company
Research Division
131 Spring Street
Lexington, MA 02173
(617) 860-3061

Dr. Robert E. Witkowski
Westinghouse Electric Corporation
1310 Beulah Road
Pittsburgh, PA 15235
(412) 256-1173

Dr. Aaron Wold
Brown University
Chemistry Department
Providence, RI 02912
(401) 863-2857

Dr. Walter A. Yarbrough
260 Materials Research Laboratory
Pennsylvania State University
University Park, PA 16802
(814) 865-2326

Mr. M. Yoder
Office of Chief of Naval Research
(ONR Code 1114SS)
800 North Quincy Street
Arlington, VA 22217-5000

Dr. Robert Pohanka (Code 1131)
Office Of Naval Research
800 N. Quincy Street
Arlington, VA 22217

Dr. David Nelson (Code 1113)
Office Of Naval Research
800 N. Quincy Street
Arlington, VA 22217

Dr. Robert W. Schwartz (Code 38505)
Naval Weapons Center
China Lake, CA 93555